

## Cu-doped TiO<sub>2</sub>-graphene/alginate nanocomposite for adsorption and photocatalytic degradation of methylene blue from aqueous solutions

Robab Mohammadi<sup>a,\*</sup>, Bakhshali Massoumi<sup>a</sup>, Behnaz Emamalinassabb<sup>a</sup>,  
Hamed Eskandarloo<sup>b</sup>

<sup>a</sup>Department of Chemistry, Payame Noor University, PO box 19395-3697, Tehran, Iran, Tel. +98 41 35421414, Fax +98 41 35431067, email: mohammadi\_rb@yahoo.com (R. Mohammadi), Tel. +98 41 35492303, Fax +98 41 35412108, email: b\_massoumi@pnu.ac.ir (B. Massoumi), Tel. +98 41 35412117, Fax +98 41 35419221, email: alinasabb@ymail.com (B. Emamalinassabb)

<sup>b</sup>School of Chemistry, College of Science, University of Tehran, Tehran, Iran, Tel. +98 21 66404647, Fax +98 21 66407719, email: eskandarloo@ut.ac.ir (H. Eskandarloo)

Received 23 September 2016; Accepted 10 May 2017

### ABSTRACT

In this study, Cu-doped TiO<sub>2</sub>-graphene/alginate (Cu-TiO<sub>2</sub>-GR/alginate) nanocomposite with high adsorption capacity and high photocatalytic activity was successfully prepared and then characterized via different analysis methods such as XRD, TEM, SEM, EDX, Raman and DRS. The photocatalytic activity and adsorption capacity of prepared nanocomposite were investigated by removal of methylene blue (MB), as a model organic pollutant, from aqueous solutions under black light irradiation. Based on results, Cu-TiO<sub>2</sub>-GR/alginate nanocomposite could effectively remove MB, and demonstrate an excellent photocatalytic enhancement over Cu-TiO<sub>2</sub> and Cu-TiO<sub>2</sub>-graphene samples. To understand the nature of adsorption process, the equilibrium adsorption isotherms were studied. The linear correlation coefficients of Langmuir, Freundlich and Temkin isotherms were obtained. Based on results, Langmuir isotherm model fitted the experimental data better than the other isotherm models. According to the Langmuir isotherm model, the maximum adsorption capacity of Cu-TiO<sub>2</sub>-GR/alginate nanocomposite for sequestering MB was about 85.95 mg. Furthermore, negative  $\Delta G^{\circ}$  and  $\Delta H^{\circ}$  values resulted from thermodynamic investigation suggested that the adsorption of MB onto Cu-TiO<sub>2</sub>-GR/alginate nanocomposite was simultaneous and exothermic in nature, respectively.

**Keywords:** Cu-TiO<sub>2</sub>-GR/alginate nanocomposite; Photocatalytic activity; Adsorption isotherms; Thermodynamic investigation; Organic pollutant

### 1. Introduction

Large volumes of wastewater are produced in manufacturing operations by the textile dyeing industry [1]. The presence of dyes in aqueous environments may cause serious environmental problems because of the toxicity of dyes to aquatic organisms and low biodegradability in such environments [2,3]. Many technologies have been applied for degradation of synthetic dyes from aqueous

solutions including membranes, adsorption/precipitation processes, integrated chemical-biological degradation, integrated iron (III) photoassisted-biological treatment, and solar photo-Fenton techniques. However, these procedures only transfer organic pollutants from liquid to solid phase, giving rise to new type of pollution and requiring further treatment [4]. Heterogeneous photocatalysis using a semiconductor has been shown to be effective for the removal of pollutants from aqueous solutions [5]. Among different semiconducting materials, titanium dioxide (TiO<sub>2</sub>) is the most commonly applied photocatalyst in environmental pollution control due to its long term photostability, inex-

\*Corresponding author.

pensiveness and safety toward both humans and the environment [1–4]. However, photocatalytic activity of  $\text{TiO}_2$  is low because of fast recombination of photogenerated electron–hole pairs [6]. Doping of a metal ion in such semiconductor can improve the trapping of electrons and prevent electron–hole recombination [7]. However, the metal selective doping is one of the key factors to increase the activity of the photocatalyst.  $\text{Cu}^{2+}$  with redox potentials of 0.16 V ( $\text{Cu}^{2+}/\text{Cu}^+$ ) and 0.52 V ( $\text{Cu}^{2+}/\text{Cu}$ ) versus the normal hydrogen electrode is considered as a good candidate for different visible-light responsive photocatalysts [8]. The electron produced from the excitation of photocatalyst is directly trapped by  $\text{Cu}^{2+}$ , which frees up the oxidative valence hole of the photocatalyst for the removal of organic compounds. Therefore, metal ions doping can provide as charge trapping sites and thus decrease electron–hole recombination rate during photocatalysis.

$\text{TiO}_2$  nanoparticles can be agglomerated easily, their aggregation influences are minimized when they are attached to the surface of various porous materials such as zeolites, silica, alumina or carbon-based materials [9–12]. More recently, graphene has attracted more interest because of its larger surface area, unique porous structure, adsorption capacity and potentially higher photocatalytic efficiencies [13]. Highly porous graphene sheets have the ability to adsorb more quantities of pollutants on their surface, and prevent selective adsorption for desired pollutants. Some functional groups such as alcohol and carboxylic acids can be remained on the graphene surface during preparation procedures [14], allowing for both adsorption of specific pollutants and attachment sites for nanoparticles to the graphene surface. Therefore, various semiconductors can be stabilized on its surface to generate more efficient photocatalysts [15]. Graphene has a conjugated structure and its combination with  $\text{TiO}_2$  can be an ideal preference to achieve an increased charge separation in electron-transfer procedures. However, few investigations have been focused on the interaction of nanoparticles and graphene sheets, and the mechanism of charge transfer between graphene and the nanocrystal. Zhang et al. [16] showed a simple method to obtain a P25-graphene nanocomposite via a one-step hydrothermal reaction for methyl blue decolorization. Farhangi et al. [17] prepared Fe- $\text{TiO}_2$ -graphene nanostructure by supercritical  $\text{CO}_2$  for photocatalytic degradation of 17 $\beta$ -estradiol ( $\text{E}_2$ ). However, the obligation to separate the nanomaterials from the suspension after treatment restricts the procedure development. The above problems can be avoided via immobilization of the nanomaterials over appropriate supports [18].

The application of immobilized nanomaterials includes several benefits such as easy separation of the adsorbent, high adsorbent density and enhancing the retention of adsorbent in the reactor [19]. Alginate is a natural polymer generated from brown algae, which has been widely applied in immobilization studies because of simple preparation, hydrophilicity and high adsorption potential to remove the pollutants [20–22]. Few researches have been focused on the graphene oxide incorporated with alginate matrix for degradation of pollutants, except for an example of graphene oxide/alginate fiber by graphene oxide as strengthening element [23]. Herein from the viewpoint of environmental friendliness, Cu- $\text{TiO}_2$ -GR was incorporated

into alginate matrixes to synthesize novel adsorbent, and we would like to further describe the possibility over the effectiveness of removal of cationic dye MB from aqueous solutions. Meanwhile, characterization of materials and relevant studies over the adsorption process and thermodynamic were also discussed.

## 2. Materials and methods

### 2.1. Materials

Titanium n-butoxide (TBOT), ethanol of absolute grade, copper (II) chloride ( $\text{CuCl}_2$ ), graphite powder (purity 99.999%), nitric acid, sulfuric acid, potassium chlorate and methylene blue were purchased from Merck Co (Germany). Sodium alginate from Laminaria hyperborean was purchased from BDH, (England).

### 2.2. Sample preparation

#### 2.2.1. Preparation of $\text{TiO}_2$ and Cu- $\text{TiO}_2$ samples

According to Refs. [24], for the preparation of  $\text{TiO}_2$  nanoparticles, a mixture of distilled water and ethanol was added drop by drop into a flask containing TBOT and ethanol. The mixture was aged for 3 h under continuous stirring at room temperature. After standing at room temperature for 24 h,  $\text{TiO}_2$  nanopowders were obtained via calcining the  $\text{TiO}_2$  xerogel at 450°C for 3 h and grinding. The molar ratio of TBOT/EtOH/ $\text{H}_2\text{O}$  was 1:29:19. For the preparation of 1.5 mol. % Cu- $\text{TiO}_2$  nanoparticles the same method was used, except that the water used in this step contained the required amount of  $\text{CuCl}_2$ .

#### 2.2.2. Preparation of graphene oxide sample

Graphene oxide was synthesized by Staudenmaier method [25]. Graphite (5 g) was reacted with concentrated nitric acid (45 mL) and sulfuric acid (90 mL) with potassium chlorate (55 g). To prevent any sudden enhancement in temperature, the potassium chlorate was added slowly over 15 min and mixture was stirred for more than 72 h at room temperature. The mixture was added to water after completing the reaction, washed with a 5% solution of HCl, and water repeatedly until the pH of the filtrate was neutral. The dried graphite oxide was placed in a quartz boat and inserted into a tubular furnace preheated to 1050°C and kept at this temperature for 30 s.

#### 2.2.3. Preparation of Cu- $\text{TiO}_2$ /GR samples

Cu- $\text{TiO}_2$ /GR catalysts with various graphene oxide contents was synthesized by hydrothermal procedure based on Zhang's work [16]. First, 5 mg of graphene oxide was dissolved in a solution of 80 mL distilled water and 40 mL ethanol via ultrasonic treatment for 2 h. Then, 200 mg of Cu- $\text{TiO}_2$  was added to the prepared graphene oxide solution and stirred for further 2 h to obtain a homogeneous suspension. Furthermore, the suspension was placed in a 200 mL Teflon-sealed autoclave at 120°C for 3 h to simultaneously get the reduction of graphene oxide and deposition of Cu-

TiO<sub>2</sub> on the graphene sheets. Finally, the obtained sample was recovered via filtration, rinsed with deionized water 10 times, and dried at 70°C for 12 h in the vacuum furnace. The prepared sample was designated as Cu-TiO<sub>2</sub>/GR<sub>1</sub>. Similar method was applied to prepare other Cu-TiO<sub>2</sub>/GR catalysts by fixing the amount of Cu-TiO<sub>2</sub> and using 10, 20 and 30 mg of graphene oxide respectively. The prepared samples were designated as Cu-TiO<sub>2</sub>/GR<sub>2</sub>, Cu-TiO<sub>2</sub>/GR<sub>3</sub>, and Cu-TiO<sub>2</sub>/GR<sub>4</sub> respectively. Finally, the best catalyst procured in this method was designated as Cu-TiO<sub>2</sub>/GR.

#### 2.2.4. Preparation of Cu-TiO<sub>2</sub>-GR/alginate sample

First, the prepared Cu-TiO<sub>2</sub>/GR sample was mixed in a 2% sodium alginate solution with a volumetric ratio of 1:2 (Cu-TiO<sub>2</sub>/GR sample: sodium alginate). The obtained mixture was stirred for 2 h to achieve homogeneity and kept for 24 h in a stable place to obtain a bubble-free concentrated solution. Then, the mixture was added dropwise by a syringe to a 0.5 mol L<sup>-1</sup> CaCl<sub>2</sub> solution with stirring. Calcium atoms can cross link and form salt bridges between the α-L-guluronic acids (G) blocks of alginate chains. As a result, Cu-TiO<sub>2</sub>/GR sample was incorporated into the alginate matrix. The resulted nanocomposite was stored in calcium chloride solution for 24 h. Finally, the nanocomposite was filtered and dried at room temperature [26].

#### 2.3. Characterization of prepared samples

The crystal phase composition and the crystallite size of prepared samples were recorded using X-ray diffraction (XRD) (Siemens/D5000) with Cu Kα radiation (0.15478 nm) in the 2θ scan range of 10°–70°. The average crystallite size (D in nm) was calculated using Scherrer's formula [21]:

$$D = \frac{k\lambda}{\beta \cos\theta} \quad (1)$$

where  $k$  is a constant equal to 0.89,  $\lambda$ , the X-ray wavelength equal to 0.154056 nm,  $\beta$ , the full width at half maximum intensity (FWHM) and  $\theta$ , the half diffraction angle. The phase content of a sample can be estimated from the integrated intensities of anatase ( $I_A$ ) and rutile ( $I_R$ ) peaks by the following equation [15]:

$$\text{Rutile phase\%} = \frac{100}{1 + 0.8 \frac{I_A}{I_R}} \quad (2)$$

Size of the prepared nanocomposite was obtained by TEM instrument (Philips CM-10 HT-100 kV). The texture and morphology of the prepared nanocomposite was measured via scanning electron microscope (SEM) (Philips XL-30ESM). The chemical composition of the synthesized nanocomposite was analyzed by an energy dispersive X-ray spectroscopy (EDX) system. Raman spectra were recorded on Takram P50C0R10 Raman spectrophotometer. Ultraviolet/visible diffuse reflectance spectra (DRS) of catalysts were performed using Avaspec-2048 TEC spectrometer in order to determine the band gap energy ( $E_g$ ) of catalysts which calculated by the following equation:

$$E_g = \frac{hc}{\lambda} = \frac{1240}{\lambda} \quad (3)$$

where,  $E_g$  is the band gap energy (eV),  $h$  is Planck's constant ( $4.1357 \times 10^{-15}$  eV),  $c$  is the light velocity ( $2.998 \times 10^8$  m s<sup>-1</sup>) and  $\lambda$  is the wavelength (nm).

#### 2.4. Studies and analysis

Removal of MB under black light irradiation was used as a model reaction to evaluate the photocatalytic activity of prepared samples. Photocatalytic activity measurements carried out at atmospheric pressure in a batch quartz reactor, as previously reported [27]. Artificial irradiation was provided by 36 W (UV-A) mercury lamp (Philips, Holland) emitted around 365 nm positioned above the batch photoreactor. In each run, 40 mg of prepared sample and 20 mg L<sup>-1</sup> of MB were fed into the quartz tube reactor and allowed to establish an adsorption-desorption equilibrium for 30 min in the darkness. The zero time reading was obtained from blank solution kept in the dark. While vigorous stirring, the reaction mixture was irradiated by black light. The residual of MB was detected by UV-vis Perkin-Elmer 550 SE spectrophotometer at wavelength of 665 nm. Experimental set-up for the adsorption of MB by Cu-TiO<sub>2</sub>-GR/alginate nanocomposite was similar to that of the photocatalytic removal of MB. However, for the batch adsorptive removal of MB by Cu-TiO<sub>2</sub>-GR/alginate nanocomposite without light irradiation, the set-up was placed inside a fully covered box in order to prevent any exposure towards light illumination. The amount of MB adsorbed onto Cu-TiO<sub>2</sub>-GR/alginate nanocomposite was calculated via Eq. (4):

$$q = \frac{(C_0 - C)V}{M} \quad (4)$$

where  $q$ ,  $C_0$  and  $C$  are the amount of adsorbed MB (mg g<sup>-1</sup>), the initial concentration and the final concentration of dye in the solution (mg L<sup>-1</sup>), respectively. In addition,  $V$  is the volume of the solution (L) and  $M$  is the weight of the nanocomposite (g) [28].

### 3. Results and discussion

#### 3.1. Characterization of prepared samples

##### 3.1.1. X-ray diffraction

XRD patterns of TiO<sub>2</sub>, Cu-TiO<sub>2</sub>, Cu-TiO<sub>2</sub>/GR and Cu-TiO<sub>2</sub>-GR/alginate samples are shown in Fig. 1. Pure anatase phase can be seen for prepared samples. In Cu-TiO<sub>2</sub>, no significant characteristic peaks of doped copper ions were detected. It may be due to low loading amount of dopant, appropriate dispersion of dopant into TiO<sub>2</sub> lattice, and its small particle size [29]. The average size of crystallites for TiO<sub>2</sub> and Cu-TiO<sub>2</sub> determined from the XRD pattern based on the Scherrer's formula were about 10 and 9 nm, respectively. Smaller crystal size obtained for Cu-TiO<sub>2</sub> nanoparticles implies that doping may decrease the crystallite growth. This reduction in particle size may be attributed to the separation of the copper ions at the grain boundary which suppresses the grain growth via restricting direct contact of grains [6]. The ionic radii of Cu<sup>2+</sup> (0.73 Å) is closer to that of Ti<sup>4+</sup> (0.68 Å). So, these ions incorporated easily into the TiO<sub>2</sub> matrix causes no crystalline dis-

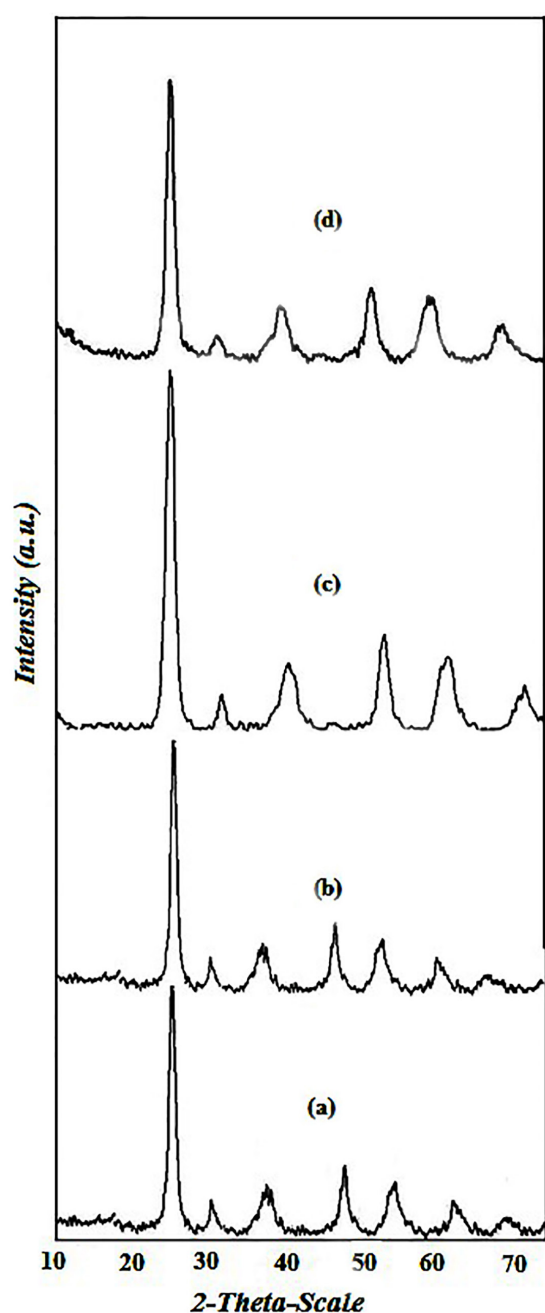


Fig. 1. XRD patterns of (a)  $\text{TiO}_2$ , (b)  $\text{Cu-TiO}_2$ , (c)  $\text{Cu-TiO}_2/\text{GR}$  and (d)  $\text{Cu-TiO}_2/\text{GR}/\text{Alginate}$ .

tortion [30]. The average crystallite size for  $\text{Cu-TiO}_2/\text{GR}$  was about 8 nm which is less than that of  $\text{Cu-TiO}_2$  sample. From Fig. 1c, the crystallinity of  $\text{Cu-TiO}_2/\text{GR}$  is higher than that of  $\text{Cu-TiO}_2$ . In explanation, when  $\text{Cu-TiO}_2$  nanostructures are grown on the surface of the graphene sheets, the functional groups on the graphene sheets act as templates, increasing crystallization and resulting in smaller sized  $\text{TiO}_2$  nanocrystals being resulted [24]. Fig. 1d shows XRD patterns of  $\text{Cu-TiO}_2/\text{GR}/\text{alginate}$  nanocomposite. The shape and the location of the peaks of  $\text{Cu-TiO}_2/\text{GR}/\text{alginate}$

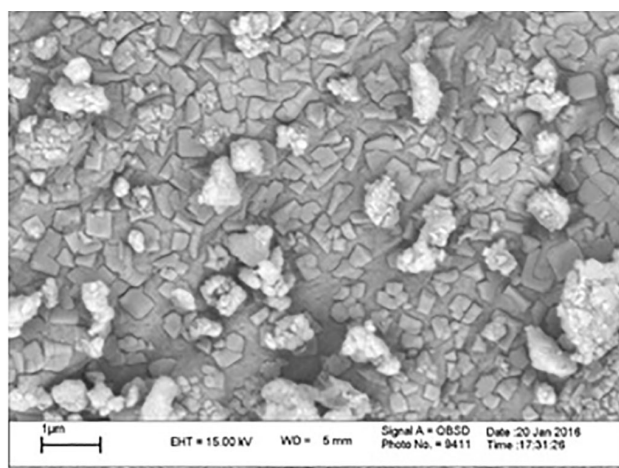


Fig. 2. SEM image of  $\text{Cu-TiO}_2/\text{GR}/\text{Alginate}$  nanocomposite.

nanocomposite and  $\text{Cu-TiO}_2/\text{GR}$  sample are the same. The process of dispersion in alginate seems to have no influence on the crystal form of  $\text{Cu-TiO}_2/\text{GR}$  sample. A small reduction in average crystallite size from 8 nm ( $\text{Cu-TiO}_2/\text{GR}$ ) to about 7 nm ( $\text{Cu-TiO}_2/\text{GR}/\text{alginate}$ ) indicated an interaction between the carboxyl groups of sodium alginate with hydroxyl groups of graphene oxide [31].

### 3.1.2. SEM Analysis of $\text{Cu-TiO}_2/\text{GR}/\text{alginate}$ nanocomposite

SEM image of  $\text{Cu-TiO}_2/\text{GR}/\text{alginate}$  nanocomposite is shown in Fig. 2. A rough structure on surface for synthesized sample can be observed from this figure. The roughened surface is suitable for sequestering pollutant molecules in aqueous phase. Also, Fig. 2 indicates  $\text{Cu-TiO}_2/\text{GR}/\text{alginate}$  nanocomposite has a highly porous structure suggests the appropriate of the nanocomposite as adsorbent for removal of MB from aqueous media.

### 3.1.3. TEM Analysis of $\text{Cu-TiO}_2/\text{GR}/\text{alginate}$ nanocomposite

Fig. 3 shows TEM image of  $\text{Cu-TiO}_2/\text{GR}/\text{alginate}$  nanocomposite. The average size of the primary particles estimated from the TEM image is about 7–10 nm, which is in good agreement with that calculated from the XRD pattern using Scherrer equation. It can be seen that the particles exhibit a relatively uniform particle size distribution. The graphene sheets can facilitate uniform dispersion of the nanoparticles on its surface.  $\text{Cu-TiO}_2$  nanoparticles grown from carboxyl groups on the surface of the graphene sheets, significantly decrease the degree of agglomeration [32].

### 3.1.4. Elemental analysis with EDX spectroscopy

Energy dispersive X-ray spectroscopy analysis was used to identify elements, which exist in the prepared  $\text{Cu-TiO}_2/\text{GR}/\text{alginate}$  nanocomposite. Cu, C, O, Na, Ca,  $\text{Cl}_2$ , and Ti peaks can be clearly seen from Fig. 4. Energy disper-

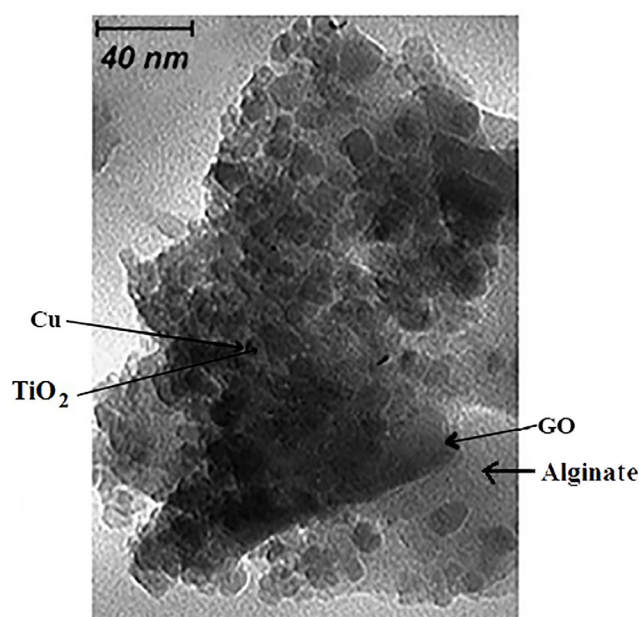


Fig. 3. TEM image of Cu-TiO<sub>2</sub>/GR/Alginate nanocomposite.

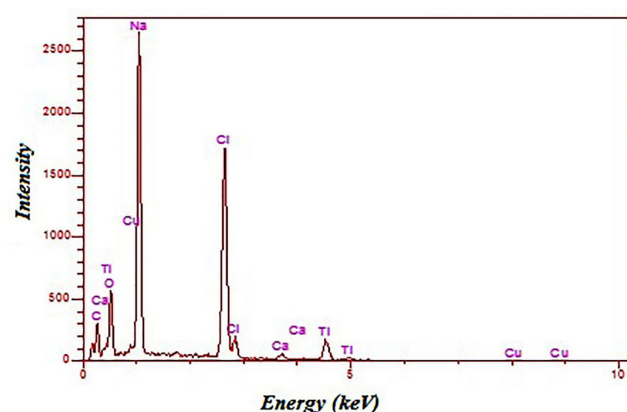


Fig. 4. EDX pattern of Cu-TiO<sub>2</sub>/GR/Alginate nanocomposite.

sive X-ray spectroscopy analysis showed no significant levels of impurities, which could have originated from the process.

### 3.1.5. Raman spectroscopy

Fig. 5 shows the Raman spectra of Cu-TiO<sub>2</sub>, Cu-TiO<sub>2</sub>/GR and pure graphene oxide (inset). The Raman spectrum of Cu-TiO<sub>2</sub> nanoparticles showed specific vibration modes located around 142 cm<sup>-1</sup> (*E<sub>g</sub>*), 392 cm<sup>-1</sup> (*B<sub>1g</sub>*), 514 cm<sup>-1</sup> (*A<sub>1g</sub>*) and 634 cm<sup>-1</sup> (*E<sub>g</sub>*), indicating the presence of anatase phase. No peak assigned to the rutile or brookite phase was observed, which is consistent with the XRD results. Also, no Cu peak is detected, which is in good accordance with the XRD patterns. The high intensity peaks indicate that Cu-TiO<sub>2</sub> nanoparticles have good crystalline nature [33]. For Cu-TiO<sub>2</sub>/GR photocatalyst, two additional prominent peaks centered at 1366 cm<sup>-1</sup> (D band) and 1592 cm<sup>-1</sup> (G band) are also observed in the Raman spectrum, suggest-

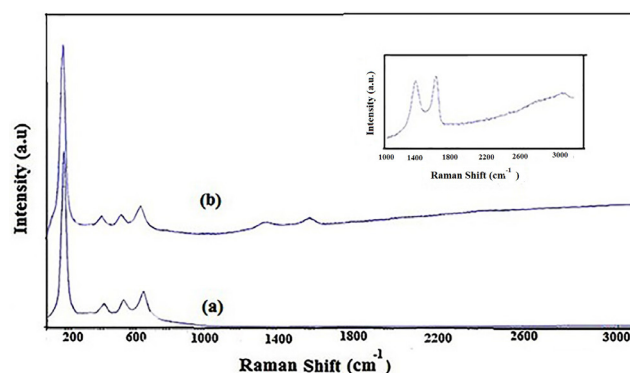


Fig. 5. Raman spectra of (a) Cu-TiO<sub>2</sub>, (b) Cu-TiO<sub>2</sub>/GR, and pure graphene oxide (inset).

ing that the structure of graphene oxide was maintained in the Cu-TiO<sub>2</sub>/GR photocatalyst. The D band is the symmetric *A<sub>1g</sub>* mode and has been attributed to the edges, defects, dangling bonds and disordered carbon, while the G band represents the *E<sub>2g</sub>* mode and corresponds to ordered sp<sup>2</sup>-bonded carbon atoms [34]. Therefore, the intensity ratio between the D and G bands (*I<sub>D</sub>*/*I<sub>G</sub>*) is a measure of the disorder, as described via the sp<sup>2</sup>/sp<sup>3</sup> carbon ratio [35]. The *I<sub>D</sub>*/*I<sub>G</sub>* values of the pure graphene oxide and Cu-TiO<sub>2</sub>/GR were calculated to be 0.93 and 0.98, suggesting that after calcination the defects in Cu-TiO<sub>2</sub>/GR were slightly enhanced because of a higher quantity of edges caused via the distortion of graphene sheets in Cu-TiO<sub>2</sub> nanoparticles [33].

### 3.1.6. DRS analysis

In order to investigate the influence of graphene oxide on the optical absorption properties of Cu-TiO<sub>2</sub> catalyst, DRS analysis has been carried out (Fig. 6). The reflectance spectra of Cu-TiO<sub>2</sub> and Cu-TiO<sub>2</sub>/GR show absorption thresholds at 408, and 442 nm, respectively, and *E<sub>s</sub>* values calculated from the Eq. (3) are 3.03, and 2.8 eV, respectively. Different studies on TiO<sub>2</sub>/graphene composites have shown that graphene sheets can narrow the band gap of TiO<sub>2</sub> [36]. These phenomenon results not only from the excellent conductivity of graphene that can facilitate separation of photogenerated charges [37], but also from the formation of Ti–O–C bonding between Cu-TiO<sub>2</sub> and graphene sheets [38]. Also, this may be attributed to the charge transfer between conduction band of TiO<sub>2</sub> catalyst and graphene sheets. However, the electron transition from the valence band to the conduction band occurs easier with the band-gap narrowing in TiO<sub>2</sub> catalyst [39]. Thus, it can be concluded that incorporation of graphene is effective for visible-light response and will play an important role for increasing the photocatalytic activity of the catalyst.

### 3.2. Photocatalytic decolorization of MB using prepared samples

Langmuir–Hinshelwood (L–H) kinetic model is widely used to explain the kinetics of photocatalytic degradation of organic pollutants in aqueous solution [40]. The L–H kinetic equation is shown in Eq. (5):

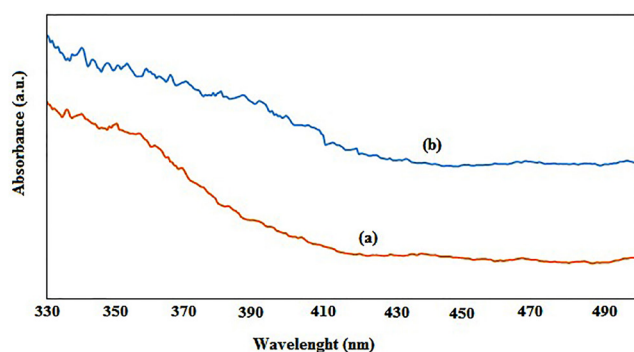


Fig. 6. UV-vis DRS spectra of (a) Cu-TiO<sub>2</sub> and (b) Cu-TiO<sub>2</sub>/GR.

$$\ln \frac{C_0}{C_t} = k_{ap} t \quad (5)$$

where  $C_0$  (mg L<sup>-1</sup>) and  $C_t$  (mg L<sup>-1</sup>) are the concentration of MB at 0 and  $t$  min, respectively. The apparent rate constant,  $k_{ap}$  (min<sup>-1</sup>), can be obtained from the slope of the versus  $t$  plot. The pseudo-first-order reaction rate constant ( $k_{ap}$ ) is chosen as the basic kinetic parameter to compare the photocatalytic activity of prepared samples. The results of decolorization of MB using synthesized samples under black light irradiation are shown in Fig. 7. It could be seen that the photocatalytic activity of Cu/TiO<sub>2</sub> nanoparticles is higher than that of the pure TiO<sub>2</sub>. It is well known that electron-hole recombination rate can be influenced by the particle size. Partial variations in particle size lead to significant modifications in the surface/bulk ratio, thus affecting the recombination rate of volume and surface electrons and holes. So, particle size can affect photocatalytic activity [27]. Cu/TiO<sub>2</sub> with smaller particle size can reduce the electron-hole recombination rate. Furthermore, a partial amount of copper ions can act as a photo-generated hole and a photo-generated electron trap and prevent the electron-hole recombination [41]. Also, Fig. 7 shows that photocatalytic activity of Cu-TiO<sub>2</sub>/GR catalyst is higher than that of Cu-TiO<sub>2</sub>. It can be concluded that interactions between graphene and Cu-TiO<sub>2</sub> lead to the improvement of the photocatalytic activity. The high photocatalytic activity of Cu-TiO<sub>2</sub>/GR samples is due to the following several factors:

1. Conduction band position of TiO<sub>2</sub> is about 3 eV (using vacuum level as a reference), and the work function of graphene is calculated to be 4.42 eV. Therefore, graphene can accept conduction band electrons from TiO<sub>2</sub>. Under excitation, the conduction band electrons of TiO<sub>2</sub> can be transferred to graphene. So, the recombination of photo-generated electron-hole pairs is efficiently prevented [42]. Therefore, the improvement in photocatalytic activity of Cu-TiO<sub>2</sub>/GR catalyst is imaginable.
2. The higher adsorption of MB onto the catalyst surface also can lead to increase the photocatalytic activity of catalyst [43]. So, when more organic molecules are adsorbed on the catalyst surface, there is a greater probability of reaction. The photo

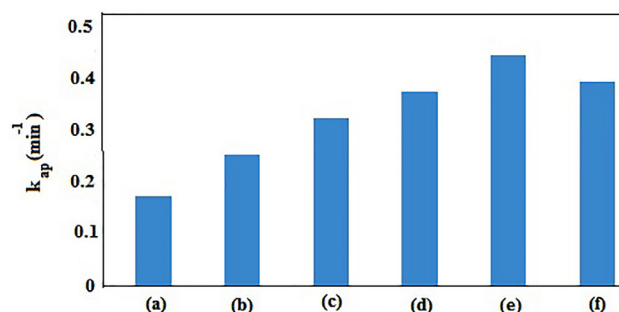


Fig. 7. Photocatalytic decolorization of MB in the presence of (a) TiO<sub>2</sub>, (b) Cu-TiO<sub>2</sub>, (c) Cu-TiO<sub>2</sub>/GR<sub>1</sub>, (d) Cu-TiO<sub>2</sub>/GR<sub>2</sub>, (e) Cu-TiO<sub>2</sub>/GR<sub>3</sub> and (f) Cu-TiO<sub>2</sub>/GR<sub>4</sub>.

generated electrons that are formed during irradiation can readily transfer to the doped copper through the graphene and then easily reduce dioxygen or other electron acceptor groups present in the aqueous medium [44,45]. As a result, electron-hole recombination is largely inhibited and this further facilitates the generation of more because of OH·: the valence band of TiO<sub>2</sub> and the superoxide radicals anion (O<sub>2</sub><sup>-</sup>) at the surface of catalyst, which in turn result in a faster

Based on the acquired results, the following mechanism would be proffered for the photocatalytic reactions [47].

1. As irradiation of TiO<sub>2</sub> with black light, valence band electrons can be excited to the conduction band. So, some holes and additional electrons are generated in the valence band and conduction band respectively.



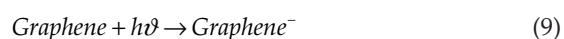
2. These excited electrons are trapped by the copper ions doped into TiO<sub>2</sub> lattice. Therefore, the recombination of electron-hole pairs is prevented.

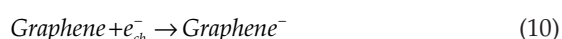


3. Molecular oxygen adsorbed on TiO<sub>2</sub> surface can scavenge the trapped electrons and generate superoxide radicals.



4. Graphene nanosheets acting as good electron acceptors [46] can accept the electrons via light illumination and the electrons excited in CB of TiO<sub>2</sub>. Therefore, the lifetime of the excited electrons and holes is prolonged, inducing higher quantum efficiency.

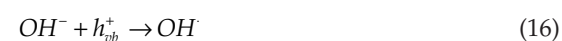
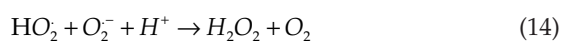




5. The positive charged hole may react with  $\text{H}_2\text{O}$  to form  $\text{OH}\cdot$ .



6. Superoxide radicals can produce other species such as hydrogen peroxide ( $\text{H}_2\text{O}_2$ ), hydroperoxy ( $\text{OH}_2\cdot$ ) and hydroxyl ( $\text{OH}\cdot$ ) radicals.



7. Finally, hydroxyl radicals can react with organic pollutants and cause the breakdowns and failures, thus convert them into minerals.



Furthermore, in Cu-TiO<sub>2</sub>/GR catalysts, the graphene content is known as an important factor in determining the photocatalytic activity. The results of decolorization of MB using Cu-TiO<sub>2</sub>/GR catalysts with various graphene contents (Cu-TiO<sub>2</sub>/GR<sub>1</sub>, Cu-TiO<sub>2</sub>/GR<sub>2</sub>, Cu-TiO<sub>2</sub>/GR<sub>3</sub> and Cu-TiO<sub>2</sub>/GR<sub>4</sub>) are illustrated in Fig. 7. From Cu-TiO<sub>2</sub>/GR<sub>1</sub> to Cu-TiO<sub>2</sub>/GR<sub>3</sub>, the photocatalytic activity was gradually increased, and Cu-TiO<sub>2</sub>/GR<sub>3</sub> demonstrated the maximized photocatalytic activity. However, when the amount of graphene is further increased above its optimum value, the photocatalytic performance deteriorates. This is ascribed to the following reasons:

1. Graphene oxide absorbs some black light and causes a light harvesting competition between Cu-TiO<sub>2</sub> and graphene. With increasing of graphene content, the photocatalytic performance is decreased [48].
2. The excessive graphene can act as a kind of recombination center instead of providing an electron pathway and promote the recombination of electron-hole pair [49].

From Fig. 8, photocatalytic activity of Cu-TiO<sub>2</sub>-GR/alginate is considerably higher than that of Cu-TiO<sub>2</sub>/GR. Cu-TiO<sub>2</sub>-GR/alginate nanocomposite became all dark blue in color, that is, MB was strongly attracted. Due to the dissociation of carboxyl groups, alginate-based photocatalyst was negatively charged and showed strong electrostatic interactions to positively charged molecules [50].

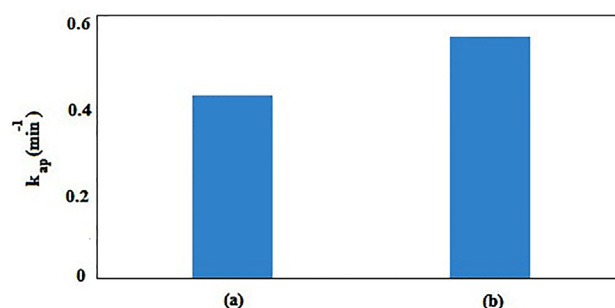


Fig. 8. Photocatalytic decolorization of MB in the presence of (a) Cu-TiO<sub>2</sub>/GR and (b) Cu-TiO<sub>2</sub>/GR/Alginate.

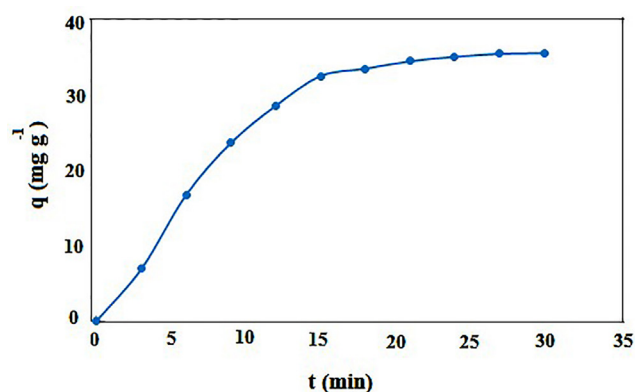


Fig. 9. Effect of contact time on MB adsorption onto Cu-TiO<sub>2</sub>/GR/Alginate nanocomposite.

### 3.3. Adsorption characteristics of Cu-TiO<sub>2</sub>-GR/alginate nanocomposite

The adsorption kinetics of MB onto Cu-TiO<sub>2</sub>-GR/alginate nanocomposite was investigated for 30 min contact time and the results are illustrated in Fig. 9. Within exposure time of 30 min, the adsorbed MB by Cu-TiO<sub>2</sub>-GR/alginate nanocomposite reached to 36.1 mg g<sup>-1</sup>. It is obvious from Fig. 9 that the increment in reaction time up to 15 min led to a little increase in adsorbed MB. The fast adsorption of MB onto Cu-TiO<sub>2</sub>-GR/alginate nanocomposite can be related to the sufficient exposure of adsorptive sites and the high surface reactivity of Cu-TiO<sub>2</sub>-GR/alginate nanocomposite for sequestering MB ions.

The results showed that the removal rate of MB by Cu-TiO<sub>2</sub>-GR/alginate nanocomposite under photocatalytic process was notably higher than the adsorption process, implying that the synergistic adsorption-photocatalysis had definitely occurred. This observation clearly revealed that during the removal of MB by Cu-TiO<sub>2</sub>-GR/alginate nanocomposite under light irradiation, both adsorption and photocatalytic processes occurred simultaneously whereby the photocatalytic process was provided by Cu-TiO<sub>2</sub>-GR while the adsorption process was contributed by alginate adsorbent. During the experiment in the dark, the rate of removal of MB via the adsorption process was calculated to be 0.245 min<sup>-1</sup>. However, when Cu-TiO<sub>2</sub>-GR/alginate

nanocomposite was exposed to light irradiation, the rate of removal of MB jumped to  $0.575 \text{ min}^{-1}$  indicating that both photocatalytic and adsorption processes manifested simultaneously.

### 3.4. Adsorption isotherm studies

In the next stage, synthesized Cu-TiO<sub>2</sub>-GR/alginate nanocomposite with the high photocatalytic activity was chosen. In order to understand the nature of adsorption process, the equilibrium adsorption isotherms were investigated. Adsorption isotherms are used to describe the interaction of solutes with adsorbent. Equilibrium adsorption isotherm data were analyzed according to the linear forms of Langmuir, Freundlich and Temkin adsorption isotherm equations (18–20), respectively [51,52]:

$$\frac{1}{q_e} = \left( \frac{1}{K_L q_m} \right) \frac{1}{C_e} + \frac{1}{q_m} \quad (18)$$

$$\ln q_e = \frac{1}{n} \ln C_e + \ln K_F \quad (19)$$

$$q_e = B_1 \ln C_e + B_2 \ln K_T \quad (20)$$

where  $C_e$  ( $\text{mg L}^{-1}$ ) is the equilibrium concentration of MB,  $q_e$  ( $\text{mg g}^{-1}$ ) is the amount of MB adsorbed at equilibrium,  $q_m$  ( $\text{mg g}^{-1}$ ) is the maximum adsorption at monolayer and  $K_L$  ( $\text{L mg}^{-1}$ ) is the Langmuir constant including the affinity of binding sites.  $K_F$  [ $\text{mg g}^{-1} (\text{L mg}^{-1})^{1/n}$ ] and  $n$  are the Freundlich constants indicating adsorption capacity and intensity, respectively.  $K_T$  ( $\text{L g}^{-1}$ ) and  $B_1$  are the Temkin constants ( $K_T$  is the equilibrium binding constant and  $B_1$  is related to the heat of adsorption). The values of Langmuir, Freundlich and Temkin parameters were calculated from the slope and intercept of linear plots of  $1/q_e$  versus  $1/C_e$ ,  $\ln q_e$  versus  $\ln C_e$  and  $q_e$  versus  $\ln C_e$ , respectively. Fig. 10 displays the adsorption isotherms plots. From the slopes and intercepts, the values of  $q_m$ ,  $K_L$ ,  $n$ ,  $K_F$ ,  $B_1$  and  $K_T$  were calculated and exhibited in Table 1.

It can be seen from Table 1 that the adsorption process could be explained by all models from comparing the results of the correlation coefficient values. However, careful observation may describe Langmuir isotherm better than others. As can be seen in Table 1, the obtained correlation coefficient for Langmuir isotherm model was higher than that of other models, which indicates the suitability of Langmuir isotherm model for describing adsorption of MB onto Cu-TiO<sub>2</sub>-GR/alginate nanocomposite. Based on Langmuir model, the maximum adsorption capacity of Cu-TiO<sub>2</sub>-GR/alginate nanocomposite for the adsorption of MB was found to be  $86.95 \text{ mg g}^{-1}$ . Essential features of Langmuir isotherm model can be expressed in term of separation factor,  $R_L$ , as below equation:

$$R_L = \frac{1}{1 + K_L C_0} \quad (21)$$

where  $C_0$  ( $\text{mg L}^{-1}$ ) is the initial dye concentration [53].

The values of  $R_L$  arranged as  $R_L = 0$ ,  $0 < R_L < 1$  and  $R_L > 1$  suggest that adsorption is irreversible, favorable and

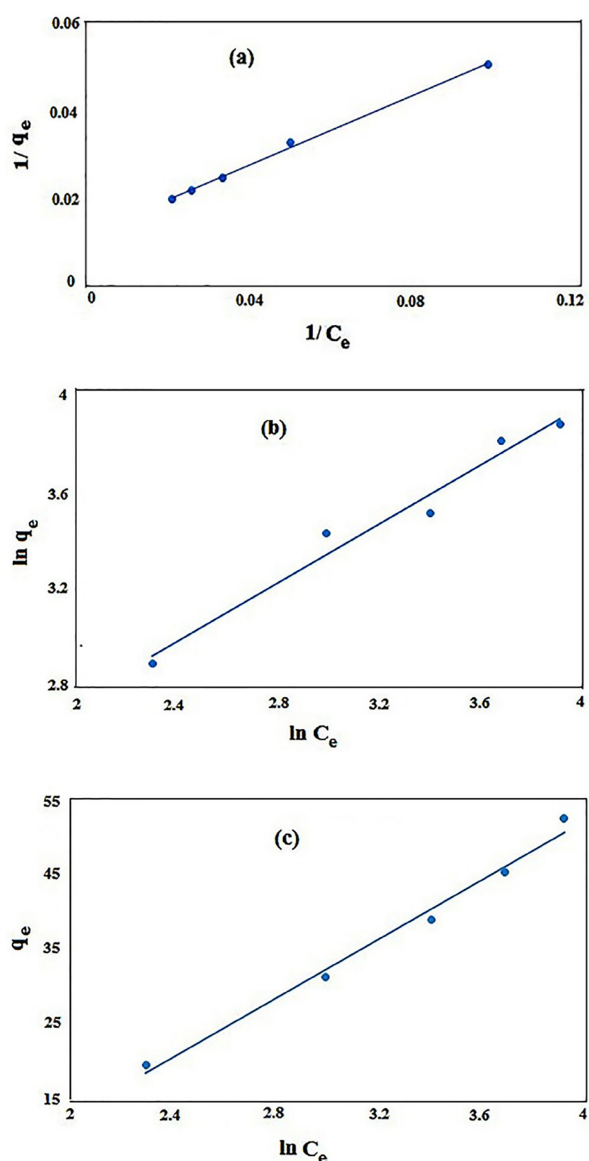


Fig. 10. Plots of linearized Langmuir (a), Freundlich (b) and Temkin (c) adsorption isotherms for MB adsorption onto Cu-TiO<sub>2</sub>/GR/Alginate nanocomposite.

unfavorable, respectively. Table 1 shows that  $R_L$  values are between 0.31 and 0.809, which indicates the adsorption of MB onto Cu-TiO<sub>2</sub>-GR /alginate nanocomposite is favorable [54].

### 3.5. Thermodynamic study

The thermodynamic study was carried out by changing the solution temperature between 25 and 40°C (298–313 K). The free energy change or Gibbs free energy ( $\Delta G^\circ$ ) ( $\text{kJ mol}^{-1}$ ), enthalpy change ( $\Delta H^\circ$ ) ( $\text{kJ mol}^{-1}$ ) and entropy change ( $\Delta S^\circ$ ) ( $\text{kJ mol}^{-1} \text{ K}^{-1}$ ) for the adsorption of MB were calculated through Eqs. (22) and (23):

$$\Delta G^\circ = -RT \ln K_D \quad (22)$$

Table 1  
Isotherm parameters for MB adsorption onto Cu-TiO<sub>2</sub>/GR/  
Alginate nanocomposite

Type of isotherm model	Value
Langmuir isotherm	
$q_m$ (mg g <sup>-1</sup> )	86.95
$K_L$ (L mg <sup>-1</sup> )	0.0283
$R_L$	0.31–0.809
$R^2$	0.9992
Freundlich isotherm	
$K_f$ (mg g <sup>-1</sup> )	4.59
$n$	1.64
$R^2$	0.9667
Temkin model	
$B_1$	20.011
$K_T$ (L g <sup>-1</sup> )	0.252
$R^2$	0.9868

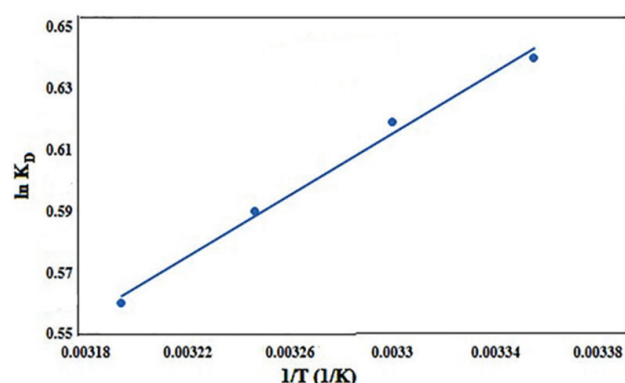


Fig. 11. Thermodynamic profile for MB adsorption onto Cu-TiO<sub>2</sub>/GR/Alginate nanocomposite.

Table 2  
Obtained parameters from thermodynamic study of MB  
adsorption onto Cu-TiO<sub>2</sub>/GR/alginate nanocomposite

Temperature (K)	( $\Delta G^0$ ) (kJ mol <sup>-1</sup> )	( $\Delta S^0$ ) (kJ mol <sup>-1</sup> K <sup>-1</sup> )	( $\Delta H^0$ ) (kJ mol <sup>-1</sup> )
298	-1.58	-0.0086	-4.16
303	-1.55	-	-
308	-1.51	-	-
313	-1.47	-	-

$$\ln K_D = \left( \frac{\Delta S^0}{R} \right) - \left( \frac{\Delta H^0}{RT} \right) \quad (23)$$

where  $R$ ,  $T$  (K) and  $K_D$  ( $q/C_e$ ) are the universal gas constant, temperature and the distribution coefficient, respectively [55]. To investigate the thermodynamic of MB adsorption onto Cu-TiO<sub>2</sub>-GR/alginate nanocomposite, thermodynamic constants such as  $\Delta G^0$ ,  $\Delta H^0$  and  $\Delta S^0$  were calculated using

Eqs. (22) and (23). From the slope ( $-\Delta H^0/R$ ) and intercept ( $\Delta S^0/R$ ) of the plot of  $\ln K_D$  versus  $1/T$ , the  $\Delta H^0$  and  $\Delta S^0$  of adsorption were estimated, respectively (Fig. 11). The values of these parameters are summarized in Table 2. Table 2 shows the negative  $\Delta G^0$  values, indicating spontaneous nature of the adsorption of MB pollutant [56]. A negative  $\Delta H^0$  indicates an exothermic adsorption process for MB pollutant. The negative value of  $\Delta S^0$  reveals the decrease of degree of freedom of adsorbed MB on the binding sites of the nanocomposite at the solid–solution interface, implying a strong binding of pollutant ions onto the active sites [57].

#### 4. Conclusion

The present study was carried out to prepare and evaluate the efficiency of Cu-TiO<sub>2</sub>-GR /alginate nanocomposite to adsorb and degrade a cationic dye (MB) from aqueous solution. The results demonstrated that Cu-TiO<sub>2</sub>-GR/alginate nanocomposite is more effective in the comparison with TiO<sub>2</sub>, Cu-TiO<sub>2</sub>, and Cu-TiO<sub>2</sub>-GR catalysts. Scanning electron microscope analysis proved a highly porous structure for Cu-TiO<sub>2</sub>-GR/alginate nanocomposite, which is suitable for sequestering pollutant molecules in aqueous phase. The average size of the primary particles estimated from the TEM image was about 7–10 nm. Among different isotherm models, the Langmuir isotherm indicated the best fit to experimental data. The obtained value for separation factor pertaining to Langmuir model indicated favorable adsorption of MB onto Cu-TiO<sub>2</sub>-GR/alginate nanocomposite. Besides, the results of thermodynamic investigation showed that the adsorption of MB via Cu-TiO<sub>2</sub>-GR/alginate nanocomposite is spontaneous and exothermic.

#### Acknowledgment

The authors acknowledge the support of the Payame Noor University of Iran.

#### References

- [1] H.R. Ebrahimi, M. Modrek, M. Mozaffari, Photo decolorization of direct red 81 (5-solamine) by using zinc oxide nanoparticles on glass granule substrate in acidic pH and various atmospheres, *World. Appl. Sci. J.*, 19 (2012) 352–354.
- [2] P. Monvisade, P. Siriphannon, Chitosan intercalated montmorillonite: preparation, characterization and cationic dye adsorption, *Appl. Clay. Sci.*, 42 (2009) 427–431.
- [3] A.R. Nestic, S.J. Velickovic, D.G. Antonovic, Characterization of chitosan/montmorillonite membranes as adsorbents for Bezactiv Orange V-3R dye, *J. Hazard. Mater.*, 210 (2012) 256–263.
- [4] R. Mohammadi, H. Eskandarloo, M. Mohammadi, Application of artificial neural network (ANN) for modeling of dyes decolorization by Sn/Zn-TiO<sub>2</sub> nanoparticles, *Desal. Water. Treat.*, 55 (2015) 1922–1933.
- [5] W. Wang, P. Serp, P. Kalck, C.G. Silva, J.L. Faria, Preparation and characterization of nanostructured MWCNT-TiO<sub>2</sub> nanocomposite materials for photocatalytic water treatment applications, *Mater. Res. Bull.*, 43 (2008) 958–967.
- [6] X. Chen, C. Burda, The electronic origin of the visible-light absorption properties of C, N and S-doped TiO<sub>2</sub> nanomaterials, *J. Am. Chem. Soc.*, 130 (2008) 5018–5019.

- [7] M. Hirano, Y. Ichihashi, Phase transformation and precipitation behavior of niobium component out of niobium-doped anatase-type TiO<sub>2</sub> nanoparticles synthesized via hydrothermal crystallization, *J. Mater. Sci.*, 44 (2009) 6135–6143.
- [8] N. Zhang, M.Q. Yang, S. Liu, Y. Sun, Y.J. Xu, Waltzing with the versatile platform of graphene to synthesize composite photocatalysts, *Chem. Rev.*, 115 (2015) 10307–10377.
- [9] C.G. Silva, R. Juarez, T. Marino, R. Molinari, H. García, Influence of excitation wavelength (UV or visible light) on the photocatalytic activity of titania containing GRId nanoparticles for the generation of hydrogen or oxygen from water, *J. Am. Chem. Soc.*, 133 (2010) 595–602.
- [10] E.P. Reddy, L. Davydov, P. Smirniotis, TiO<sub>2</sub>-loaded zeolites and mesoporous materials in the sonophotocatalytic decomposition of aqueous organic pollutants: the role of the support, *Appl. Catal. B: Environ.*, 42 (2003) 1–11.
- [11] N. Farhangi, S. Ayissi, P.A. Charpentier, Fe doped TiO<sub>2</sub>-graphene nanostructures: synthesis, DFT modeling and photocatalysis, *Nanotechnol.*, 25 (2014) 305601–305611.
- [12] M.J. Sampaio, C.G. Silva, A.M.T. Silva, L.M. Pastrana-Martínez, C. Han, Carbon-based TiO<sub>2</sub> materials for the degradation of microcystin-LA, *Appl. Catal. B: Environ.*, 170 (2015) 74–82.
- [13] C. Han, N. Zhang, Y.J. Xu, Structural diversity of Graphene materials and their multifarious roles in heterogeneous photocatalysis, *Nano Today*, 11 (2016) 351–372.
- [14] G. Williams, B. Seger, P.V. Kamat, TiO<sub>2</sub>-Graphene nanocomposites. UV-assisted photocatalytic reduction of Graphene oxide, *ACS nano.*, 2 (2008) 1487–1491.
- [15] R. Hasan, C.W. Lai, S.B.A. Hamid, W.J. Basirun, Z. Lockman, F. Bari, Photoelectrocatalytic activity of Zn-loaded RGR-TiO<sub>2</sub> nanocomposite coatings on mild steel substrate via DC electrochemical co-deposition, *Eur. Phys. J. Appl. Phys.*, 65 (2014) 20303 p1–20303 p8.
- [16] H. Zhang, X. Lv, Y. Li, Y. Wang, J. Li, P25-Graphene nanocomposite as a high performance photocatalyst, *ACS Nano.*, 4 (2010) 380–386.
- [17] N. Farhangi, R.R. Chowdhury, Y. Medina-GRnzalez, M.B. Ray, P.A. Charpentier, Visible light active Fe doped TiO<sub>2</sub> nanowires grown on Graphene using supercritical CO<sub>2</sub>, *Appl. Catal. B: Environ.*, 110 (2011) 25–32.
- [18] X. Zhao, L. Lv, B. Pan, W. Zhang, S. Zhang, Q. Zhang, Polymer-supported nanocomposites for environmental application: a review, *Chem. Eng. J.*, 170 (2011) 381–394.
- [19] T.G. Luan, J. Jin, S.M.N. Chan, Y.S. Wong, N.F.Y. Tam, Biosorption and biodegradation of tributyltin (TBT) by alginate immobilized *Chlorella vulgaris* beads in several treatment cycles, *Process. Biochem.*, 41 (2006) 1560–1565.
- [20] Y.N. Mata, M.L. Blazquez, A. Ballester, F. GRnzalez, J.A. Munoz, Biosorption of cadmium, lead and copper with calcium alginate xerogels and immobilized *Fucus vesiculosus*, *J. Hazard. Mater.*, 163 (2009) 555–562.
- [21] N. Rangsayatorn, P. Pokethitiyook, E.S. Upatham, G.R. Lanza, Cadmium biosorption by cells of *Spirulina platensis* TISTR 8217 immobilized in alginate and silica gel, *Environ. Int.*, 30 (2004) 57–63.
- [22] A. Bee, D. Talbot, S. Abramson, V. Dupuis, Magnetic alginate beads for Pb(II) ions removal from wastewater, *J. Colloid. Interface. Sci.*, 362 (2011) 486–492.
- [23] Y. He, N. Zhang, Q. GRng, H. Qiu, W. Wang, Y. Liu, J. Gao, Alginate/graphene oxide fibers with enhanced mechanical strength prepared by wet spinning, *Carbohydr. Polym.*, 88 (2012) 1100–1108.
- [24] R. Mohammadi, B. Massoumi, H. Eskandarloo, Preparation and characterization of Sn/Zn/TiO<sub>2</sub> photocatalyst for enhanced amoxicillin trihydrate degradation, *Desal. Water. Treat.*, 53 (2015) 1995–2004.
- [25] L. Staudenmaier, Verfahren zur Darstellung der GRaphitsäure, *Ber. Dtsch. Chem. Ges.*, 31 (1898) 1481–1487.
- [26] Y.N. Mata, M.L. Blazquez, A. Ballester, F. GRnzalez, J.A. Munoz, Biosorption of cadmium, lead and copper with calcium alginate xerogels and immobilized *Fucus vesiculosus*, *J. Hazard. Mater.*, 163 (2009) 555–62.
- [27] R. Mohammadi, Influence of preparation method on the physicochemical properties and catalytic activity of SiO<sub>2</sub>-TiO<sub>2</sub> mixed oxides, *Desal. Water. Treat.*, 57 (2016) 22370–22377.
- [28] R.D.C. Soltani, A. Rezaee, G.S. Khorramabadi, K. Yaghmaeian, Optimization of lead(II) biosorption in an aqueous solution using chemically modified aerobic digested sludge, *Water. Sci. Technol.*, 63 (2011) 129–135.
- [29] H.B. Huang, D.Y.C. Leung, Complete elimination of indoor formaldehyde over supported Pt catalysts with extremely low Pt content at ambient temperature, *J. Catal.*, 280 (2011) 60–67.
- [30] K.H. Ko, Y.C. Lee, Y.J. Jung, Enhanced efficiency of dye-sensitized TiO<sub>2</sub> solar cells (DSSC) by doping of metal ions, *J. Colloid. Interface. Sci.*, 283 (2005) 482–487.
- [31] G. Yang, L. Zhang, T. Peng, W. Zhong, Effects of Ca<sup>2+</sup> bridge cross-linking on structure and pervaporation of cellulose/alginate blend membranes, *J. Membr. Sci.*, 175 (2000) 53–60.
- [32] K.P. Loh, Q. Bao, G. Eda, M. Chhowalla, Graphene oxide as a chemically tunable platform for optical applications, *Nature. Chem.*, 2 (2010) 1015–1024.
- [33] P.K. Dubey, P. Tripathi, R.S. Tiwari, A.S.K. Sinha, O.N. Srivastava, Synthesis of reduced Graphene oxidee TiO<sub>2</sub> nanoparticle composite systems and its application in hydrogen production, *Int. J. Hydrogen Energy*, 39 (2014) 16282–16292.
- [34] L. Zhang, Q. Zhang, H. Xie, J. Guo, H. Lyu, Y. Li, Z. Sun, H. Wang, Z. Guo, Electrospun titania nanofibers segregated by Graphene oxide for improved visible light photocatalysis, *Appl. Catal. B: Environ.*, 201 (2017) 470–478.
- [35] A. Morais, C. Longr, J.R. Araujo, M. Barroso, J.R. Durrant, A.F. Nogueira, Nanocrystalline anatase TiO<sub>2</sub>/reduced Graphene oxide composite films as photoanodes for photoelectrochemical water splitting studies: the role of reduced Graphene oxide, *Phys. Chem. Phys.*, 18 (2016) 2608–2016.
- [36] Q. Zhang, Y. He, X. Chen, D. Hu, L. Li, T. Yin, L. Ji, Structure and photocatalytic properties of TiO<sub>2</sub>-Graphene oxide intercalated composite, *Chine. Sci. Bull.*, 56 (2011) 331–339.
- [37] D. Yang, A. Velamakanni, G. Bozoklu, S. Park, M. Stoller, R.D. Piner, S. Stankovich, I. Jung, D.A. Field, C.A. Ventrone, R.S. Ruoff, Chemical analysis of Graphene oxide films after heat and chemical treatments by X-ray photoelectron and Micro-Raman spectroscopy, *Carbon*, 47 (2009) 145–152.
- [38] H. Zhang, X. Lv, Y. Li, Y. Wang, J. Li, P25-Graphene composite as a high performance photocatalyst, *ACS Nano.*, 4 (2010) 380–386.
- [39] M.Q. Yang, Y.J. Xu, Photocatalytic conversion of CO<sub>2</sub> over Graphene-based composites: current status and future perspective, *Nanoscale Horiz.*, 1 (2016) 185–200.
- [40] K. Guan, Relationship between photocatalytic activity, hydrophilicity and self-cleaning effect of TiO<sub>2</sub>/SiO<sub>2</sub> films, *Surf. Coat. Technol.*, 191 (2005) 155–160.
- [41] R. Mohammadi, B. Massoumi, M. Rabani, Photocatalytic decomposition of amoxicillin trihydrate antibiotic in aqueous solutions under UV irradiation using Sn/TiO<sub>2</sub> nanoparticles, *Int. J. Photoenergy*, 2012 (2012) 1–11, ID 514856.
- [42] N. Zhang, Y.J. Xu, The endeavour to advance graphene-semiconductor composite-based photocatalysis.
- [43] J.C. Sin, S.M. Lam, K.T. Lee, A.R. Mohamed, Preparation and photocatalytic properties of visible light-driven samarium-doped ZnO nanorods, *Ceram. Int.*, 39 (2013) 5833–5843.
- [44] Y. Zhang, Z.R. Tang, X. Fu, Y.J. Xu, TiO<sub>2</sub>-Graphene nanocomposites for gas-phase photocatalytic degradation of volatile aromatic pollutant: is TiO<sub>2</sub>-graphene truly different from other TiO<sub>2</sub>-carbon composite materials?, *ACS Nano.*, 4 (2010) 7303–7314.
- [45] Y. Zhang, Z.R. Tang, X. Fu, Y.J. Xu, Engineering the Unique 2D Mat of Graphene to Achieve Graphene-TiO<sub>2</sub> Nanocomposite for Photocatalytic Selective Transformation: What Advantage does Graphene Have over Its Forebear Carbon Nanotube?, *ACS Nano.*, 5 (2011) 7426–7435.
- [46] R.M. Mohamed, UV-assisted photocatalytic synthesis of TiO<sub>2</sub>-reduced Graphene oxide with enhanced photocatalytic activity in decomposition of sarin in gas phase, *Desal. Water. Treat.*, 50 (2012) 147–156.

- [47] D.G. Huang, S.J. Liao, W.B. Zhou, S.Q. Quan, L. Liu, Z.J. He, J.B. Wan, Synthesis of samarium- and nitrogen-co-doped TiO<sub>2</sub> by modified hydrothermal method and its photocatalytic performance for the deGRadation of 4-chlorophenol, *J. Phys. Chem. Solids*, 70 (2009) 853–859.
- [48] T.G. Xu, L.W. Zhang, H.Y. Cheng, Y.F. Zhu, Significantly enhanced photocatalytic performance of ZnO via Graphene hybridization and the mechanism study, *Appl. Catal. B: Environ.*, 101 (2011) 382–387.
- [49] G. Zhu, T. Xu, T. Lv, L.K. Pan, Q.F. Zhao, Z. Sun, Graphene incorporated nanocrystalline TiO<sub>2</sub> films for CdS quantum dot-sensitized solar cells, *J. Electroanal. Chem.*, 650 (2011) 248–251.
- [50] Y.B. Lin, B. Fugetsu, N. Terui, S. Tanaka, Removal of organic compounds by alginate gel beads with entrapped activated carbon, *J. Hazard. Mater.*, 120 (2005) 237–241.
- [51] E.M. Seftel, M. Niarchos, C. Mitropoulos, M. Mertens, E.F. Vansant, P. Cool, Photocatalytic removal of phenol and methylene-blue in aqueous media using TiO<sub>2</sub>@LDH clay nanocomposites, *Catal. Today*, 252 (2015) 120–127.
- [52] A. Mehrizad, K. Zare, H. Aghaie, S. Dastmalchi, Removal of 4-chloro-2-nitrophenol occurring in drug and pesticide waste by adsorption onto nano-titanium dioxide, *Int. J. Environ. Sci. Technol.*, 9 (2012) 355–360.
- [53] L. Zhou, J. Jin, Z. Liu, X. Liang, C. Shang, Adsorption of acid dyes from aqueous solutions by the ethylenediamine-modified magnetic chitosan nanoparticles, *J. Hazard. Mater.*, 185 (2011) 1045–1052.
- [54] R.D.C. Soltani, A.R. Khataee, M. Safari, S.W. Joo, Preparation of bio-silica/chitosan nanocomposite for adsorption of a textile dye in aqueous solutions, *Int. Biodeter. BiodeGR.*, 85 (2013) 383–391.
- [55] G.J. Copello, A.M. Mebert, M. Raineri, M.P. Pesenti, L.E. Diaz, Removal of dyes from water using chitosan hydrogel/SiO<sub>2</sub> and chitin hydrogel/SiO<sub>2</sub> hybrid materials obtained by the sol-gel method, *J. Hazard. Mater.*, 186 (2011) 932–939.
- [56] L. Fan, C. Luo, M. Sun, X. Li, H. Qiu, Highly selective adsorption of lead ions by water-dispersible magnetic chitosan/Graphene oxide nanocomposites, *Coll. Surf. B.*, 103 (2013) 523–529.
- [57] A. Rahmani, H.Z. Mousavi, M. Fazli, Effect of nanostructure alumina on adsorption of heavy metals, *Desalination*, 253 (2010) 94–100.